Synchrotron X-ray Scattering Study of the Mechanism of Nanopore Generation in Nanoporous Organosilicate Thin Films Imprinted with a Reactive Six-Armed Porogen

Kyuyoung Heo,[†,‡] Kyeong Sik Jin,[†,‡] Weontae Oh,[‡,§] Jinhwan Yoon,[†] Sangwoo Jin,[†] and Moonhor Ree*[,†]

Department of Chemistry, National Research Lab for Polymer Synthesis & Physics, Pohang Accelerator Laboratory, Center for Integrated Molecular Systems, Polymer Research Institute, and BK School of Molecular Science, Pohang University of Science and Technology (Postech), Pohang 790-784, Republic of Korea, and Department of Nanotechnology, Dong-Eui University, 955 Eomgwangno, Busanjin-gu, Busan 614-714, Republic of Korea

Received: March 6, 2006; In Final Form: June 20, 2006

In situ grazing incidence small-angle X-ray scattering analysis was successfully performed during the thermal processing of film blends of polymethylsilsesquioxane (PMSSQ) precursor and triethoxysilyl-terminated six-arm poly(ϵ-caprolactone) (mPCL6) porogen. In addition, thermogravimetric analysis of the films was carried out in a nitrogen atmosphere. These measurements provide important information about the structures of the blend films and of the resulting porous films. In particular, they are used in this paper to establish the mechanism of the formation of imprinted pores within the blend films. During the heating run, the sacrificial thermal degradation of the porogen component commenced at 320 °C, generating pores in the resulting cured PMSSQ films. Only very limited porogen aggregation occurred during the blend film formation process (spin-coating and subsequent drying), and these porogen aggregates were of relatively small size and narrow size distribution. The observed restriction of the formation of such porogen aggregates was found to result from the favorable hybridization reaction of the porogen's reactive end groups with the reactive functional groups of the PMSSQ precursor, which competes with aggregation via reaction between the porogen molecules. The average radius (or half-size) of the porogen aggregates was in the range 2.45−3.98 nm, depending on the porogen loading (10−40 wt %). The porogen aggregates retained their size and size distribution until thermal degradation, which resulted in the imprinting of nanopores in the cured PMSSQ films with size and size distribution corresponding to those of the porogen aggregates. The porosities of the resulting nanoporous films were in the range 12.4−41.7%, depending on the initial porogen loading.

Introduction

Scaling down the feature size of integrated circuits (ICs), i.e., reducing the cross sections of interconnects, is always accompanied by significant increases in the resistance of metal conductor wiring and in the capacitance between interconnects, which result in significant crosstalk and capacitive coupling and thus in increased power dissipation.[1,2] For this reason, the microelectronics industry is currently attempting to replace traditional aluminum wiring and SiO_2-based insulators (dielectric constant k of 4.0−4.5) with highly conductive copper wiring and low dielectric constant (low-k) interdielectric materials ($k \ll 2.5$).[1−3] Low-k dielectrics can not only lower line-to-line noise in interconnect conductors but also minimize power dissipation by reducing the capacitance between the interconnects,[1−3] and thus there is strong demand for such materials in the microelectronics industry.

Most dielectric materials reported so far have k values greater than 2.5.[4−6] Air is known to have $k = 1.0$, which is the lowest value attainable. There has been much interest in incorporating nanoscale voids into dielectric materials in order to reduce their k value and thus in producing low-k porous interdielectric materials.[4,7] One approach to the development of low-k porous dielectric materials is the templated polycondensation of soluble organosilicate precursors in the presence of a thermally labile, organic polymeric porogen: voids are formed in the resulting dielectrics through the thermal decomposition of the porogens.[8−12] However, the tendency of porogens to aggregate in organosilicates has limited reduction of the pore size and porosity of the resulting dielectrics,[8−12] making them unsuitable for use in advanced ICs patterned with small feature sizes.

In particular, the large number of arms of star-shape porogens has been found to result in severe aggregation, even with a 10 wt % porogen loading, generating both large-sized and interconnected pores in dielectric thin films.[9−12] The development of advanced ICs requires a method for generating dielectric materials with a uniform distribution of closed pores that have dimensions significantly smaller than the feature size. Moreover, the ability to characterize the pore structures of porous dielectric thin films is as important as developing appropriate dielectrics and porogens. Last, understanding the mechanism of pore generation in such dielectric materials is vital for progress in this area.

Therefore, in the present study we have chosen triethoxysilyl-terminated six-armed poly(ϵ-caprolactone) (mPCL6) as a reac-

* To whom correspondence should be addressed. E-mail: ree@postech.edu. Tel: +82-54-279-2120. Fax: +82-54-279-3399.

† Department of Chemistry, National Research Lab for Polymer Synthesis & Physics, Pohang Accelerator Laboratory, Center for Integrated Molecular Systems, Polymer Research Institute, and BK School of Molecular Science, Pohang University of Science and Technology.

‡ These authors contributed equally to this work.

§ Department of Nanotechnology, Dong-Eui University.

10.1021/jp061372i CCC: $33.50
Published on Web 07/21/2006

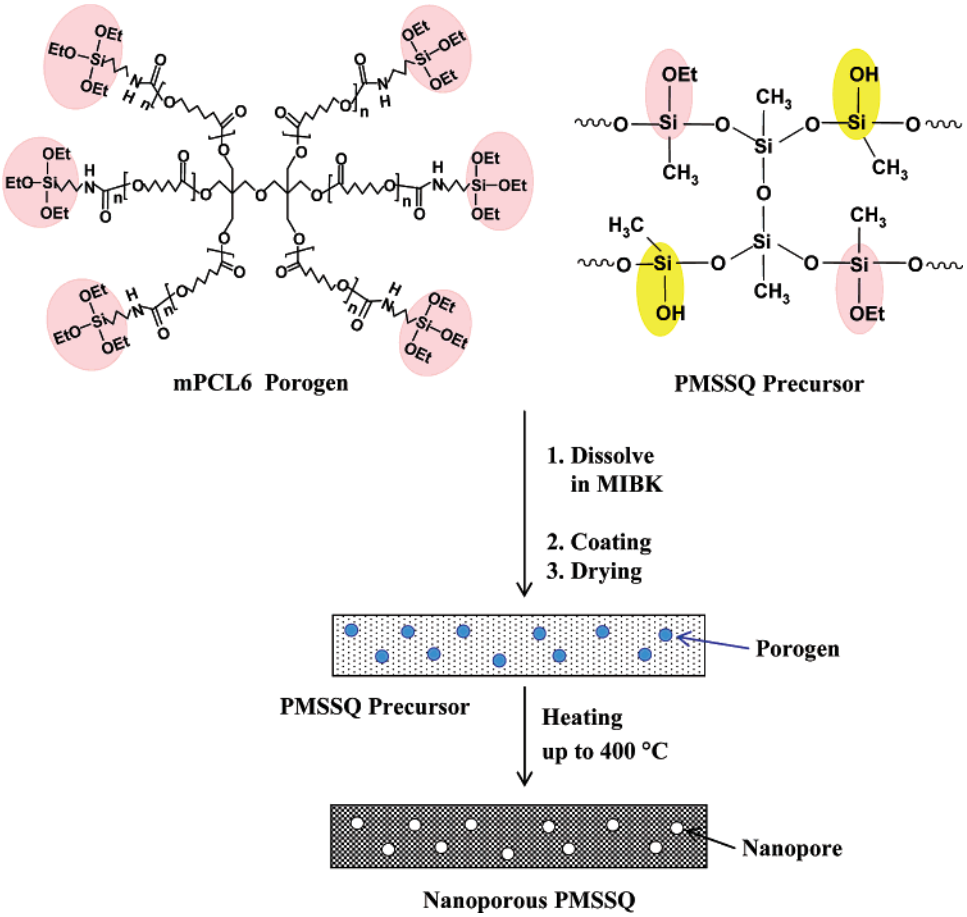

Figure 1. Procedure for the preparation on nanoporous dielectric thin films from the PMSSQ precusor (curable dielectric matrix) and triethoxysilyl-terminated star-shaped PCL porogen (mPCL6, thermally labile porogen).

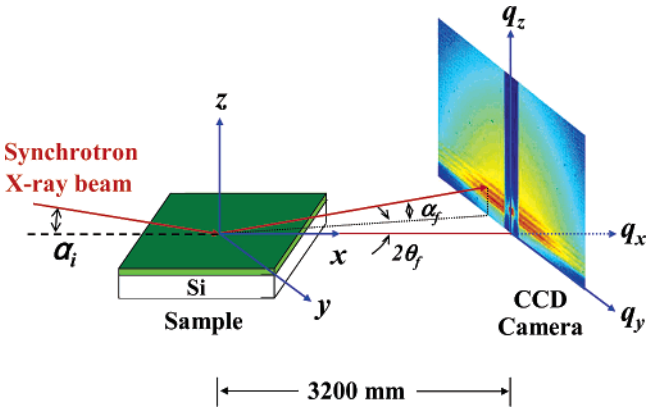

Figure 2. Geometry of grazing incidence small-angle X-ray scattering (GISAXS). An incident X-ray beam impinges on the surface of a thin film at an angle α_i and then the scattered pattern is measured on a two-dimensional charge-coupled detector (2D CCD), where α_f is the exit angle with respect to the film surface and $2\theta_f$ is the scattering angle with respect to the plane of incidence.

tive model porogen and polymethylsilsesquioxane (PMSSQ) precursor as a soluble organosilicate dielectric precursor (Figure 1) and quantitatively investigated the mechanism of thermal nanopore imprinting in nanometer-scale thin films of the PMSSQ dielectric loaded with the mPCL6 porogen by using in situ grazing incidence small-angle X-ray scattering (GISAXS) with synchrotron X-ray radiation sources (Figure 2) and thermogravimetric analysis (TGA). As seen in Figure 1, the triethoxysilyl terminal groups on the mPCL6 porogen are analogues of the reactive functional groups (ethoxysilyl and hydroxysilyl) of the PMSSQ precursor that take part in the curing reaction (i.e., the secondary polycondensation reaction) during heat-treatment. Due to the similarity of the two types of groups, the porogen can be more miscible with the PMSSQ precursor and, furthermore, the triethoxysilyl groups can cause the porogen to participate in the curing reaction of the PMSSQ precursor, leading to a significant inhibition or reduction of aggregation in their blend films. The in situ GISAXS and TGA analysis of this study has established the mechanism of thermal pore generation in thin films of mPCL6 porogen and PMSSQ precursor mixtures. This study has further highlighted the potential of triethoxysilyl-modification of end groups as a means of preventing or reducing severe aggregation of star-shape and dendritic porogens with large numbers of arms in the preparation of low-*k* nanoporous organosilicate dielectric films. In addition, the present study has demonstrated the power of the GISAXS technique as a tool for characterizing the pore shape, size, and size distribution, as well as the electron density and porosity, in nanoporous dielectric thin films of nanoscale thickness.

Experimental Section

A soluble polymethylsilsesquioxane (PMSSQ) precursor with a weight-average molecular weight, $\overline{M}_w$, of 10000 and containing ethoxy and hydroxyl groups (GR650F)[6] was supplied by Techneglas Company (Perrysburg, OH). A triethoxysilyl-terminated six-arm poly(ϵ-caprolactone) (mPCL6) porogen was synthesized and found to have a $\overline{M}_w$ of 9600 and a polydispersity index of 1.11.[12]

A series of homogeneous solutions of the mPCL6 porogen and PMSSQ precursor in dry methyl isobutyl ketone (MIBK)

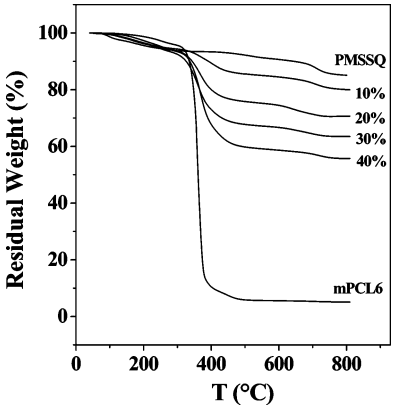

Figure 3. TGA thermograms of the PMSSQ precursor, the mPCL6 porogen, and the PMSSQ precusor/mPCL6 porogen composites. The measurements were carried out at a heating rate of 2.0 °C/min under a nitrogen atmosphere.

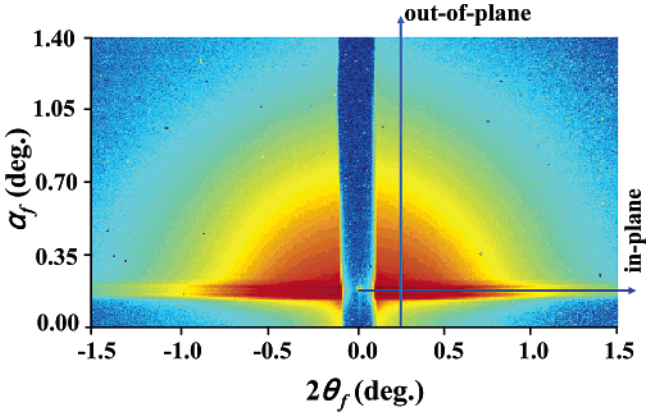

Figure 4. 2D GISAXS pattern measured at $\alpha_i = 0.20°$ for a 100 nm thick porous film derived from a PMSSQ precursor film loaded with 20 wt % mPCL6.

(5 wt % solid) were prepared using porogen compositions of 10, 20, 30, and 40 wt %. Each solution was filtered with a PTFE-membrane microfilter of pore size 0.20 μm, spin-coated onto precleaned Si(100) wafers, and then dried at 50 °C for 1 h under a nitrogen atmosphere. The thicknesses of the dried films were found to be in the range 100−150 nm by using a spectroscopic ellipsometer (model VASE, Woollam, Lincoln, NE).

TGA measurements were performed at 2.0 °C/min in a nitrogen atmosphere using a Seiko TG/DT analyzer (model EXSTAR 6000 TG/DT, Seiko Instruments, Japan). In situ GISAXS measurements were carried out at the 4C1 and 4C2 beam lines at the Pohang Light Source (PLS).[13] A monochromatized X-ray radiation source of $\lambda = 0.171$ nm (λ, wavelength) and a two-dimensional charge-coupled device (2D CCD) detector (Roper Scientific, Trenton, NJ) were used. The sample-to-detector distance was 3200 mm. Aluminum foil strips were employed as semitransparent beam stops because the intensity of the specular reflection from the substrate is much stronger than the intensity of GISAXS near the critical angle. Each film sample was mounted on a homemade *z*-axis goniometer equipped with a vacuum chamber. The incidence angle α_i of each X-ray beam was set in the range 0.20−0.22°, which is between the critical angles of the films and the Si(100) substrate ($\alpha_{c,f}$ and $\alpha_{c,s}$) (Figure 2). The film sample was heated to 400 °C at a rate of 2.0 °C/min and kept at that temperature for 30 min under vacuum. Thereafter, the films were cooled to room temperature at a rate of 2.0 °C/min under vacuum. Each measurement was collected for 145 s. Data correction was carried out with respect to the background scattering and the intensity decay of the incident primary X-rays during measurements. Scattering angles were corrected for the variations in the positions of the X-ray beams reflected from the silicon substrate interface with changes in the incidence angle α_i and by a precalibrated polystyrene-*b*-polyethylene-*b*-polybutadiene-*b*-polystyrene copolymer. In addition, transmission electron microscopy (TEM) measurements were carried out using a JEM microscope (model 4000Fx) on samples prepared on carbon grids of 400 mesh by dip-coating in dilute solutions (1.0 wt % solid content).

Results and Discussion

Figure 3 shows the TGA thermograms of the mPCL6 porogen, PMSSQ precursor, and their blends in various compositions, which were obtained by heating at 2.0 °C/min in a nitrogen atmosphere over the range 30−800 °C.

As can be seen in this figure, the mPCL6 porogen undergoes some weight loss in the temperature range 83−320 °C due to the evaporation of ethanol byproduct generated by the thermal curing reaction of the porogen's triethoxysilyl terminal groups, and significant weight loss occurs above 320 °C as a result of thermal decomposition. Similar weight loss behaviors were observed for mPCL6 porogen molecules loaded into a PMSSQ precursor matrix. This onset temperature of thermal degradation ($T_{d,p}$) is much higher than that (246 °C) of the corresponding unmodified PCL6 porogen and that of the unmodified PCL6 porogen loaded in a PMSSQ precursor matrix (291 °C).

The PMSSQ precursor also undergoes weight loss in the temperature range 75−340 °C, which is attributed to the evaporation of the water and ethanol byproducts generated by the thermal curing reaction of the precursor's hydroxysilyl and ethoxysilyl end groups, and very slow thermal decomposition of the cured PMSSQ dielectric occurs above 500 °C (Figure 3).

These TGA results indicate that during the heating run both the mPCL6 porogen and the PMSSQ precursor components of the blend films undergo curing reactions in the temperature range 83−320 °C prior to the sacrificial thermal decomposition of the porogen component. This concurrence of the curing reactions of the porogen and precursor matrix components favors the chemical hybridization of the components, which prevents the formation of large porogen aggregates.

For nanoscale thin films of blends of the mPCL6 porogen and PMSSQ precursor with various compositions, in situ GISAXS measurements were carried out. A representative two-dimensional (2D) GISAXS pattern is presented in Figure 4. For each measured 2D GISAXS pattern, one-dimensional (1D) in-plane and out-of-plane GISAXS profiles were extracted at $\alpha_f = 0.17°$ and $2\theta_f = 0.25°$, respectively, where α_f is the angle between the scattered beam and the film surface, and $2\theta_f$ is the angle between the scattered beam and the plane of incidence (Figure 4). Representative in-plane GISAXS profiles are displayed in Figure 5, which were extracted from the 2D GISAXS patterns measured in situ during heating at 2.0 °C/min of a PMSSQ precursor film loaded with 10 wt % mPCL6. As can be seen in this figure, the dried PMSSQ precursor film containing 10 wt % mPCL6 porogen has a structural featured scattering profile, but its intensity is relatively weak, which is attributed to the relatively weak contrast between the electron densities of the PMSSQ precursor and the porogen. The scattering profile retains its shape up to 320 °C (=$T_{d,p}$, the onset temperature of porogen thermal degradation) and even above $T_{d,p}$. The scattering intensity varies very little with increasing

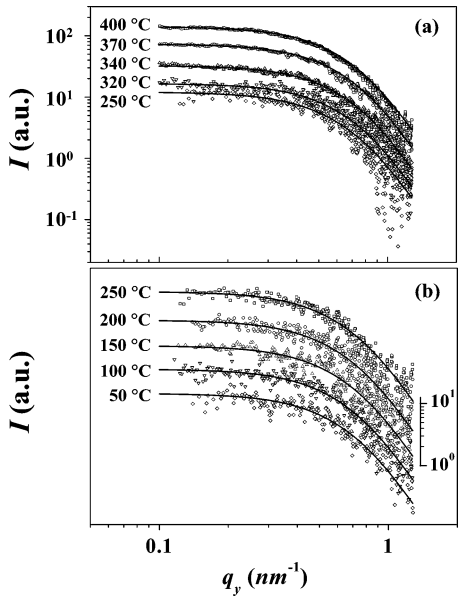

Figure 5. (a, b) In-plane GISAXS profiles at $\alpha_f = 0.17°$ of 2D GISAXS patterns measured during heating (2.0 °C/min) of a PMSSQ precursor film loaded with 10 wt % mPCL6 under vacuum. The symbols represent the measured data, and the solid lines were obtained by fitting the data with the GISAXS formula of a sphere model.

temperature up to 320 °C, and thereafter increases with temperature because of the pores created in the film by the thermal degradation of the porogen molecules. Similar sets of in-plane scattering profiles were obtained for PMSSQ precursor films loaded with more than 10 wt % mPCL6 (data not shown).

We attempted to quantitatively analyze the in-plane scattering profiles with the following recently derived GISAXS formula[11,14]

$$I_{\mathrm{GISAXS}}(\alpha_f, 2\theta_f) \cong \frac{1}{16\pi^2}\frac{1-e^{-2\mathrm{Im}(q_z)d}}{2\mathrm{Im}(q_z)} \cdot \begin{bmatrix} |T_i T_f|^2 I_1(q_{||}, \mathrm{Re}(q_{1,z})) + \\ |T_i R_f|^2 I_1(q_{||}, \mathrm{Re}(q_{2,z})) + \\ |T_f R_i|^2 I_1(q_{||}, \mathrm{Re}(q_{3,z})) + \\ |R_i R_f|^2 I_1(q_{||}, \mathrm{Re}(q_{4,z})) \end{bmatrix} \quad (1)$$

where $\mathrm{Im}(q_z) = |\mathrm{Im}(k_{z,f})| + |\mathrm{Im}(k_{z,i})|$, Re($x$) is the real part of x, d is the film thickness, R_i and T_i are the reflected and transmitted amplitudes of the incoming X-ray beam, respectively, and R_f and T_f are the reflected and transmitted amplitudes of the outgoing X-ray beam, respectively. $q_{1,z} = k_{z,f} - k_{z,i}$, $q_{2,z} = -k_{z,f} - k_{z,i}$, $q_{3,z} = k_{z,f} + k_{z,i}$, $q_{4,z} = -k_{z,f} + k_{z,i}$, and $q_{||} = \sqrt{q_x^2 + q_y^2}$. Here, $k_{z,i}$ is the z-component of the wave vector of the incoming X-ray beam, which is given by $k_{z,i} = k_o\sqrt{n_R^2 - \cos^2 a_i}$, and $k_{z,f}$ is the z-component of the wave vector of the outgoing X-ray beam, which is given by $k_{z,f} = k_o\sqrt{n_R^2 - \cos^2 a_f}$, where $k_o = -2\pi/\lambda$, λ is the wavelength of the X-ray beam, and n_R is the refractive index of the film given by $n_R = 1 - \delta + i\beta$ with a dispersion δ and an absorption β. I_1 is the scattering intensity of the porogens or pores in the film, which can be calculated kinematically.

To analyze the scattering profiles by using the above GISAXS formula, we examined all possible scattering models (for example, sphere, ellipsoid, cylinder, and so on) for the scattered intensity from structures in the film (i.e., I_1 term in eq 1), and then found that a sphere model is the most suitable for porogens or their imprinted pores in the films prepared with 10 wt % porogen loading, which is expressed in the following equation:

$$I_1 = c\int_0^\infty n(r)v^2(r)|F(qr)|^2 S(qr)\,\mathrm{d}r \quad (2)$$

where c is a constant, $v(r)$ is the volume of each pore, $F(qr)$ is the spherical form factor, and $S(qr)$ is the structure factor for the monodisperse hard sphere model.[15] $n(r)$ is the log-normal size distribution function of the porogens or pores

$$n(r) = \frac{1}{\sqrt{2\pi}\, r_o \sigma e^{\sigma^2/2}} e^{-\ln(r/r_o)^2/2\sigma^2} \quad (3)$$

where r is the porogen (or pore) radius, and r_0 and σ are the radius corresponding to the peak maximum and the width of the radius distribution of the porogens (or pores), respectively.

As can be seen in Figure 5, all these scattering profiles can be satisfactorily fitted with the GISAXS formula in combination with eqs 2 and 3. These results indicate that the porogen molecules (or porogen aggregates) in the film and the imprinted pores in the resulting porous film are spherical and have a sharp interface with the matrix component. In these fittings we considered all possible packing structures for the structure factor $S(qr)$ and then found that only a randomly packed structure of spheres well fits the scattering data, informing that the porogen molecules (or porogen aggregates), as well as their imprinted pores are randomly dispersed in the film.

TABLE 1: Results of Analysis of in-Plane GISAXS Profiles Measured in Situ during Heating Runs of PMSSQ Precursor/mPCL6 Porogen Composite Films up to 400 °C and Subsequent Cooling Runs of the Resulting Porous Films

	10 wt % porogen loading pore size and size distribution			20 wt % porogen loading pore size and size distribution		
temp (°C)	r_o (nm)	σ	$\bar{r}$ (nm)	r_o (nm)	σ	$\bar{r}$ (nm)
on heating						
50	2.10	0.32	2.45	2.35	0.41	3.02
100	2.11	0.32	2.46	2.35	0.41	3.02
120	2.11	0.32	2.46	2.41	0.41	3.10
150	2.11	0.32	2.46	2.41	0.41	3.10
200	2.11	0.32	2.46	2.41	0.41	3.10
250	2.07	0.33	2.44	2.41	0.41	3.10
320	2.10	0.33	2.47	2.40	0.42	3.13
340	2.10	0.33	2.47	2.41	0.42	3.14
370	2.10	0.33	2.47	2.40	0.42	3.13
400	2.09	0.33	2.46	2.40	0.42	3.13
on cooling						
25	2.17	0.32	2.53	2.40	0.42	3.13

The results of the analyses of these scattering profiles are summarized in Table 1 and Figure 6. It was found that the mPCL porogen component of the film has $\bar{r}$ (average radius) = 2.45−2.47 nm with $\sigma = 0.32-0.33$ for the range 50−320 °C. These radius values and radius distribution widths are slightly larger than those ($\bar{r} = 1.86$ nm and $\sigma = 0.28$) of the single porogen molecule, which were estimated from the molecular weight using a relationship reported in the literature.[16] These results indicate that even in a PMSSQ precursor film loaded with 10 wt % mPCL6 porogen, limited aggregation of the porogen molecules takes place during the film formation process, i.e., spin-casting and subsequent drying at 50 °C in a nitrogen atmosphere, and that the resulting porogen aggregates retain their size and size distribution until they undergo thermal degradation (Table 1 and Figure 6).

From the analysis of the scattering profiles obtained above 320 °C, the size and size distribution of the pores imprinted in

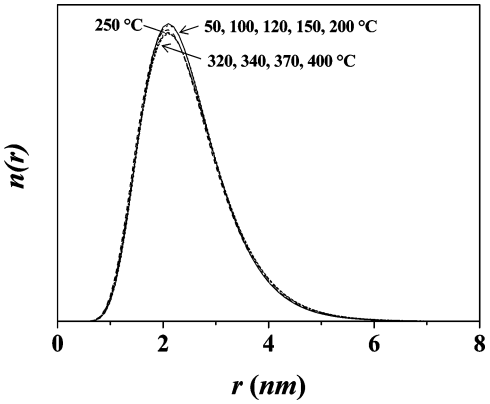

Figure 6. Pore radius and distribution determined from the GISAXS analysis of the in-plane scattering profile data in Figure 5.

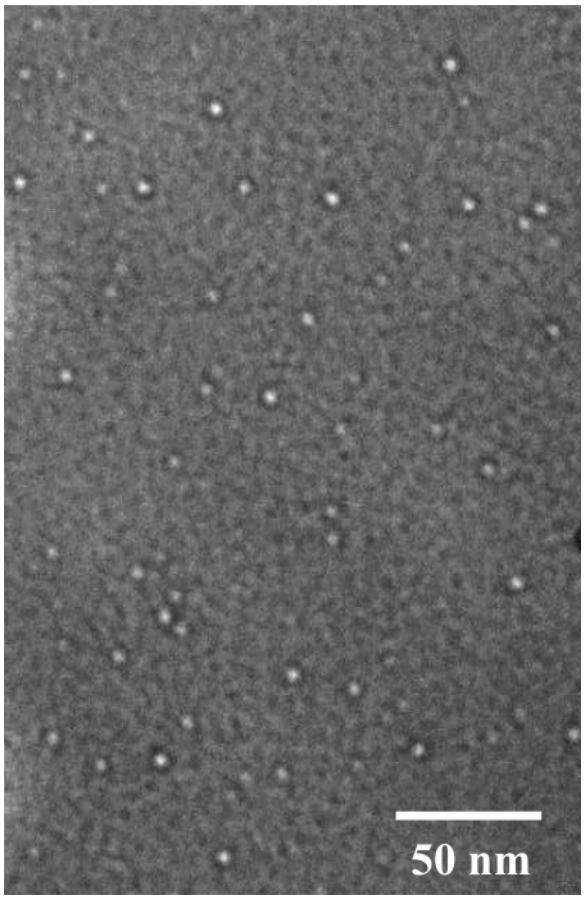

Figure 7. TEM image of a nanoporous PMSSQ dielectric prepared from a PMSSQ precursor sample loaded with 10.0 wt % mPCL6 porogen.

the film were found to be almost identical to those of the porogen aggregates that developed during the film formation process (Table 1 and Figure 6). These results indicate that above 320 °C the porogen aggregates within the immobilized PMSSQ precursor matrix undergo sacrificial thermal firing without further aggregation. Thus the imprinted pores have sizes equivalent to those of the porogen aggregates.

This spherical structure and the randomly dispersed spheres determined by the GISAXS analysis were confirmed by TEM analysis. A representative TEM image of a porous PMSSQ film is shown in Figure 7. This TEM image clearly shows that the pores generated in the dielectric film by the sacrificial thermal degradation of the mPCL6 porogen are spherical in shape. However, it is noted that in the blend the porogen molecules or their aggregates in spherical shape prior to sacrificial thermal firing could not easily be identified by TEM analysis because their low electron density contrast with respect to that of the PMSSQ precursor matrix.

TABLE 2: Results of Analysis of in-Plane GISAXS Profiles Measured in Situ during Heating Runs of PMSSQ Precursor/mPCL6 Porogen Composite Films up to 400 °C and Subsequent Cooling Runs of the Resulting Porous Films

	30 wt % porogen loading pore size and size distribution			40 wt % porogen loading pore size and size distribution		
temp (°C)	r_o (nm)	σ	$\bar{r}$ (nm)	ξ (nm)	σ	$(\bar{l}_p/2)$ (nm)
on heating						
50	2.90	0.46	3.98	4.53	−[a]	3.89
100	2.91	0.46	4.00	4.63	−	3.97
120	2.96	0.47	4.12	4.63	−	3.97
150	3.00	0.47	4.18	4.50	−	3.86
200	3.00	0.47	4.18	4.50	−	3.86
250	2.99	0.47	4.16	4.45	−	3.82
320	2.99	0.48	4.24	4.29	−	3.68
340	2.99	0.48	4.24	4.29	−	3.68
370	2.99	0.49	4.29	4.99	−	4.28
400	2.98	0.48	4.21	4.92	−	4.22
on cooling						
25	2.98	0.48	4.21	4.99	−	4.28

[a] Not obtainable from the analysis with the Debye's random two-phase model.

The quantitative scattering data analysis with the GISAXS formula was extended to the in-plane scattering profiles obtained for the PMSSQ precursor films loaded with 20 and 30 wt % mPCL6 porogen during the heating runs. All the scattering profiles could be satisfactorily fitted with the GISAXS formula (data not shown). The data analysis results are summarized in Tables 1 and 2. As can be seen in this table, the PMSSQ precursor films loaded with 20 and 30 wt % mPCL6 porogen were found to have aggregates of the porogen molecules with the same size and size distribution as observed for the film containing 10 wt % porogen. The porogen aggregates were found to retain their size and size distribution without any further aggregation up to $T_{d,p}$ (=320 °C) and then to sacrificially decompose above 320 °C, resulting in the imprinting of nanopores with the same size and size distribution as the porogen aggregates, as was observed for the film containing 10 wt % porogen.

The higher loadings of the mPCL6 porogen in the PMSSQ precursor film result in larger aggregates of the porogen molecules with a broader size distribution, and thus in larger nanopores with a broader size distribution, $\bar{r}$ and σ are in the ranges 2.44−2.47 nm and 0.32−0.33, respectively, for the 10 wt % porogen loaded film, 3.02−3.14 nm and 0.41−0.42, respectively, for the 20 wt % porogen loaded film, and 3.98−4.29 nm and 0.46−0.49, respectively, for the 30 wt % porogen loaded film (Table 2).

In contrast to the results for these films, the in-plane scattering profiles of the films containing 40 wt % mPCL6 porogen could not be fitted using the GISAXS formula with eqs 2 and 3. We examined other possible models for the scattered intensity I_1. We found that Debye's random two-phase model[17,18] provided the best description of I_1 for analyzing the scattering profiles of films prepared with 40 wt % porogen loading

$$I_1 = \frac{8\pi\phi(1-\phi)(\rho_{e(PMSSQ)} - \rho_{e(porogen\ or\ pore)})^2\xi^3}{(1+q^2\xi^2)^2} \quad (4)$$

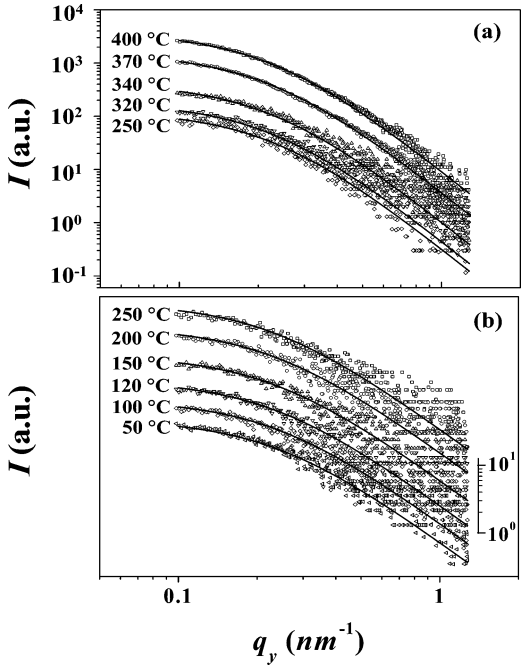

Figure 8. (a, b) In-plane GISAXS profiles at $\alpha_f = 0.17°$ of 2D GISAXS patterns measured during heating (2.0 °C/min) of a PMSSQ precursor film loaded with 40 wt % mPCL6 under vacuum. The symbols represent the measured data, and the solid lines were obtained by fitting the data with the GISAXS formula of a random two-phase Debye model.

where ϕ and $(1 - \phi)$ are the volume fractions of the porogen aggregates (or pores) and PMSSQ matrix component in the film respectively, ρ_i is the electron density of component i, and ξ is the correlation length defined by $1/\xi = 1/\bar{l}_p + 1/\bar{l}_{PMSSQ}$ where $\bar{l}_p$ and $\bar{l}_{PMSSQ}$ are the mean chord lengths of the porogen aggregate (or pore) and PMSSQ phase, respectively. Here, the average size $\bar{l}_p$ of the porogen aggregates or pores can be obtained from the determined ξ value using the relation $\bar{l}_p = \xi/(1 - \phi)$.

As shown in Figure 8, all the scattering profiles could be fitted with the GISAXS formula for a random two-phase structure. These results indicate that the porogen aggregates in the film and the imprinted pores in the resulting porous film have a random shape, which is different to the spherical shapes of the porogen aggregates and imprinted pores observed in films prepared with porogen loadings up to 30 wt %. Irregular porogen aggregates and imprinted pores might result from the formation of interconnected porogen aggregates. In particular, a certain degree of interconnection between the porogen aggregates might occur during the film formation process (solution casting and subsequent drying).

The results of the analyses of the scattering profiles are summarized in Table 2. The scattering data analysis found that the mPCL porogen component in the film forms aggregates with $\bar{l}_p/2 = 3.68-3.89$ nm in the temperature range 50−320 °C and the pores imprinted above 320 °C have a size of $\bar{l}_p/2 = 3.68-4.28$ nm. These results can be summarized as follows. The pores imprinted in the film with 40 wt % porogen have a random shape rather than the spherical shape observed for the pores imprinted in the films with ≤30 wt % porogen loadings. However, the sizes of the porogen aggregates and the imprinted pores are comparable to those of the spherical pores imprinted in PMSSQ dielectric films imprinted with 30 wt % porogen. Moreover, the sizes of the pores imprinted in the film were found to be almost identical to those of the porogen aggregates developed during the film formation process, as was also observed in the films loaded with ≤30 wt % porogen.

The above results provide important information about the mechanism of nanopore generation in the porous PMSSQ films. The mPCL6 porogen was successfully loaded at concentrations up to 40 wt % into the PMSSQ precursor matrix without any severe phase separation. Only limited phase separation took place during solution casting and drying in the blend film formation process, leading to small porogen aggregates with a narrow size distribution in the dried films. The sizes and size distributions of the porogen aggregates were found to vary slightly depending on the porogen loading; overall, a larger porogen loading resulted in the formation of slightly larger porogen aggregates. The porogen aggregates were found to have a spherical shape in the films prepared with porogen loadings up to 30 wt % but irregular shapes in films loaded with 40 wt % porogen. The porogen aggregates retained their size and size distribution without any further aggregation until thermal degradation, resulting in the imprinting of nanopores in the cured PMSSQ films with sizes and size distributions corresponding to those of the porogen aggregates.

This limited aggregation behavior of mPCL porogen and its high PMSSQ precursor matrix loading capability are attributed to the reactive triethoxysilyl end groups of the porogen, which can react with the reactive functional groups (i.e., the ethoxysilyl and hydroxysilyl groups) of the PMSSQ precursor. These groups can react during the blend film formation process. Two competing reactions can occur: (i) hybridization reaction between the porogen and PMSSQ precursor and (ii) aggregation of the porogen molecules. As described above, limited aggregation of the porogen molecules was observed in the dried blend films, which is evidence that both reactions occurred in the blend film formation process. The limitation of aggregation indicates that the chemical fixation of the porogen molecules onto the PMSSQ precursor molecules via hybridization reaction occurs more favorably than porogen aggregation. Such hybridization reaction is favored during thermal processing because of the overlapping of the temperature regions in which the curing reactions of the porogen and the PMSSQ precursor occur, as discussed above in the section on TGA analysis; consequently this hybridization reaction prevents any further porogen aggregation from occurring during the thermal processing of the dried blend film. Thus the reactive triethoxysilyl end groups of the porogen play a major role in minimizing aggregation of the porogen molecules in the PMSSQ dielectric throughout the entire film formation process, including spin-casting, drying, curing of the precursor polymer, and the thermal decomposition of the porogen.

From the experimental in-plane GISAXS profiles, the invariant Q values were determined: Q is the integrated area of a scattering profile with respect to the measured q range, which is proportional to the product of the volume fractions of the PMSSQ and porogen (or pore) components and to the difference between the squared electron densities of the two components of the film.[13,19] The resulting invariant Q values are plotted in Figure 9. As can be seen in this figure, Q is small at room temperature and is independent of the porogen loading as well as of the degree of porogen aggregation in the PMSSQ precursor films, which is principally due to the weak contrast between the electron densities of the porogen and PMSSQ precursor components. However, Q increases very slowly with increases in temperature during the heating run. Q increases rapidly around 320 °C ($=T_{d,p}$), and continues to rise up to 400 °C. These results provide important information about films in which porogen

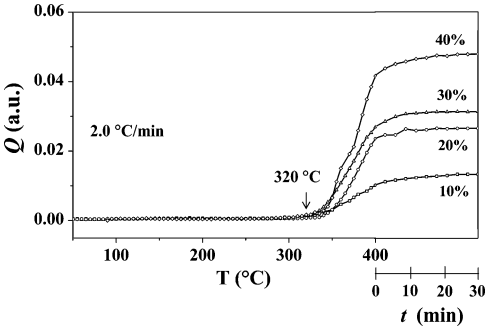

Figure 9. Invariants from the in-plane GISAXS profiles during the heating run. After 400 °C, subsequent thermal treatment continued at 400 °C for 30 min. Here, the *Q* values can be regarded as representing the overall scattering power of the sample that takes into account the intensity of scattering that is expected from it under all possible scattering geometry.

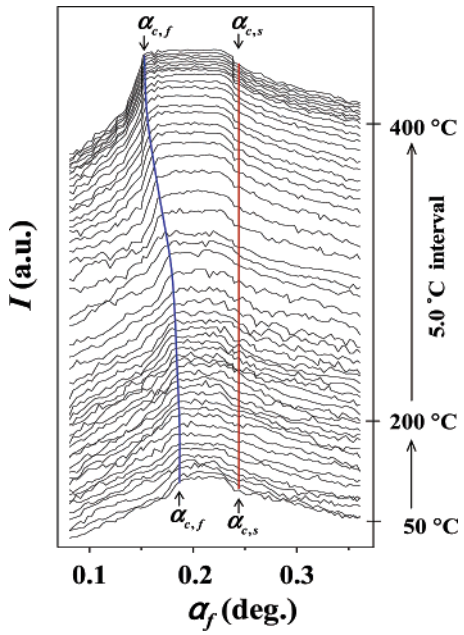

Figure 10. Out-of-plane GISAXS profiles at $2\theta_f = 0.25°$ of 2D GISAXS patterns measured during heating (2.0 °C/min) of a PMSSQ precursor film loaded with 30 wt % mPCL6 under vacuum. $\alpha_{c,f}$ and $\alpha_{c,s}$ indicate the critical angle of the film and the silicon substrate, respectively.

aggregates undergo sacrificial thermal degradation, generating pores, and the PMSSQ precursor undergoes curing. These results are in good agreement with the TGA results described above.

Figure 10 shows a representative set of out-of-plane GISAXS profiles, which were extracted at $2\theta_f = 0.25°$ from the 2D GISAXS patterns measured in situ during heating at 2.0 °C/min of a PMSSQ precursor film loaded with 30 wt % mPCL6 porogen. As can be seen in this figure, the scattering profile obtained at 50 °C is very weak, which is attributed to the weak electron density contrast between the porogen and PMSSQ precursor components. From this scattering profile, the critical angle of the film $\alpha_{c,f}$ was estimated to be 0.185°; the critical angle of the silicon substrate $\alpha_{c,s}$ is 0.245°. With increases in temperature, a variation of $\alpha_{c,f}$ is clearly evident, but $\alpha_{c,s}$ does not appear to vary. $\alpha_{c,f}$ decreases slowly as the temperature approaches 320 °C. This is due to the removal of water and ethyl alcohol, which are formed in the film as byproducts of the curing of the PMSSQ precursor component. Above 320 °C, $\alpha_{c,f}$ decreases significantly as the temperature is increased, reaching a final value of 0.151° at 400 °C. This drastic shift in

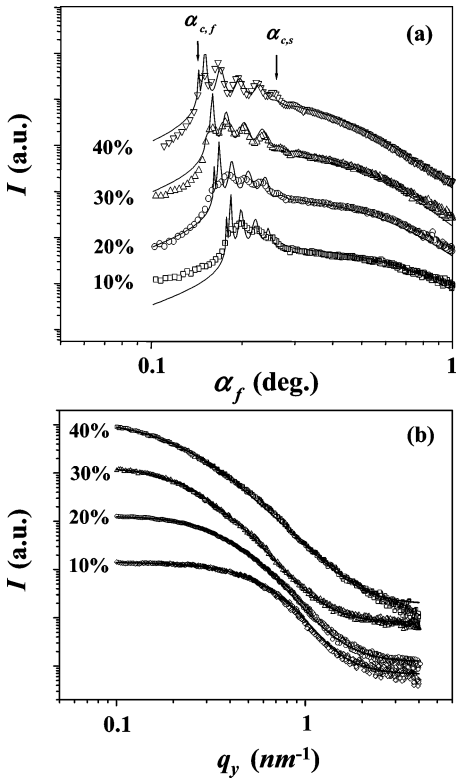

Figure 11. (a) Out-of-plane GISAXS profiles obtained at $2\theta_f = 0.25°$ from 2D GISAXS patterns of porous PMSSQ films imprinted by the mPCL6 porogen. (b) In-plane GISAXS profiles at $\alpha_f = 0.17°$ of 2D GISAXS patterns measured for nanoporous PMSSQ films imprinted with mPCL6 porogen. The porous film samples are labeled according to the initial porogen loading in weight percent. The symbols are the measured data, and the solid lines were obtained by fitting the data with the GISAXS formula. $\alpha_{c,f}$ and $\alpha_{c,s}$ are the critical angles of the film and the silicon substrate, respectively.

$\alpha_{c,f}$ is attributed primarily to the reduction in the electron density of the film that occurs when pores are imprinted in the film as a result of the thermal degradation of the porogen aggregates but also to the removal of the water and ethyl alcohol byproducts from the film. Similar trends in $\alpha_{c,f}$ with temperature were observed for the out-of-plane GISAXS profiles of the films with other compositions (data not shown).

The experimental out-of-plane GISAXS profiles were further analyzed in detail with the GISAXS formula and by using the structural parameters of the films obtained from the analysis of the in-plane GISAXS profiles. Some of the results of this analysis are presented in Figure 10. As can be seen in Figure 11a, the scattering profiles of the films imprinted with 10−30 wt % mPCL6 porogen loadings can be satisfactorily fitted with the GISAXS formula by using eqs 2 and 3 and the pore parameters obtained from the in-plane scattering data analysis (Figure 11b). The scattering profiles of the films imprinted with 40 wt % mPCL6 porogen loadings can be satisfactorily fitted with the GISAXS formula by using eq 4 and the pore parameters obtained from the in-plane scattering data analysis. These results confirm that the pore size and pore size distribution are isotropic in- and out-of-plane within the dielectric films. Moreover, the out-of-plane scattering profiles in Figure 11a show that the critical angle $\alpha_{c,f}$ of the porous films decreases with increases in the initial porogen loading. This trend results from the decrease in the electron density of the resulting porous films. From the determined $\alpha_{c,f}$ values, the electron densities of the porous films $\rho_{e,f}$ were calculated using the following relationship between $\alpha_{c,f}$ and $\rho_{e,f}$: $\rho_{e,f} = \pi\alpha_{c,f}^2/r_e\lambda^2$, where r_e is the classical

TABLE 3: Pore Structures and Properties of Nanoporous PMSSQ Dielectric Thin Films Imprinted with mPCL6 Porogen

porogen loading (wt %)	$\alpha_{c,f}$ (deg)	ρ_e (nm^{-3})	P (%)
0	0.185	396	0
10	0.173	347	12.4
20	0.162	305	23.0
30	0.151	265	33.1
40	0.141	231	41.7

radius (2.818×10^{-15} m) of the electron and λ is the wavelength of the X-ray beam.[10] Further, the porosities of the porous films with respect to that of the PMSSQ film with no porogen loading were estimated from these $\rho_{e,f}$ values. The results are summarized in Table 3. The porosities of the porous films were found to be in the range 12.4−41.7%, depending on the initial porogen loading; higher initial porogen loadings of the PMSSQ precursor film resulted in porous dielectric films with higher porosities.

Conclusions

A series of blend films of mPCL porogen and PMSSQ precursor in various compositions were prepared onto silicon substrates by conventional spin-coating their homogeneous solutions and subsequent drying and investigated in detail during thermal process with a heating rate of 2.0 °C/min by using GISAXS and TGA analysis. These analyses established the mechanism of the formation of imprinted pores within the blend films. Moreover, the GISAXS data analysis provided important information about the structures of the blend films and of the resulting porous films.

The loading of mPCL6 porogen into the PMSSQ precursor matrix was carried out successfully up to 40 wt % without any severe porogen aggregation. It was found that only limited phase separation took place during the blend film formation process (spin-coating and subsequent drying process), producing porogen aggregates of small size and narrow size distribution in the resulting blend films.

The porogen aggregates were found to have a spherical shape in the films prepared with porogen loadings up to 30 wt % but irregular shapes in films loaded with 40 wt % porogen. The average radius (or half-size) of porogen aggregates was in the range 2.45−3.98 nm, depending on the porogen loading. The observed restriction of the formation of such porogen aggregates was found to result from the favorable hybridization reaction of the porogen's reactive triethoxysilyl end groups with the reactive functional groups of the PMSSQ precursor, which competes with the porogen aggregation that occurs via the condensation of the porogen molecules.

The porogen aggregates commenced sacrificial thermal degradation at 320 °C in the thermal process, and ultimately left their individual footprints in the film as nanopores. The nanopore size and size distribution were identical to those of the porogen aggregates prior to thermal degradation. Further, the sizes and size distributions of the imprinted pores were isotropic in- and out-of-plane within the films as observed in the blend films prior to thermal degradation. Higher initial porogen loadings in the PMSSQ precursor films resulted in dielectric films with higher porosities; the porosities ranged 12.4−41.7%, depending on the initial porogen loading in the range 10−40 wt %.

In conclusion, the reactive triethoxysilyl terminal groups of the porogen play a major role in minimizing the aggregation of the porogen molecules in the PMSSQ dielectric throughout the entire film formation process, including spin-casting, drying, curing of the precursor polymer, and the thermal decomposition of the porogen.

In addition, this study demonstrated that in situ GISAXS is a powerful tool for monitoring the thermal nanopore templating process in the formation of nanoporous dielectric thin films, providing structural characteristics as a function of thin film process parameters such as temperature and time.

Acknowledgment. This work was supported by the National Research Lab (NRL) Program (Contract No. 2005-01385) and the Science Research Center (SRC) Program (Center for Integrated Molecular Systems at Postech) of the Korea Science and Engineering Foundation (KOSEF) and by the Korean Ministry of Education (Brain Korea 21 Program). Synchrotron GISAXS measurements were supported by the Ministry of Science and Technology and POSCO.

References and Notes

(1) *The International Technology Roadmap for Semiconductors*; Semiconductor Industry Association: San Jose, CA, 2004

(2) Czornyj, G.; Chen, K. R.; Pradasilva, G.; Arnold, A.; Souleotis, H.; Kim, S.; Ree, M.; Volksen, W.; Dawson, D.; DiPietro, R. *Proc. Electron. Compon. Technol. Conf.* **1992**, *42*, 682.

(3) Miller, R. D. *Science* **1999**, *286*, 421.

(4) (a) Ree, M.; Yoon, J.; Heo, K. *J. Mater. Chem.* **2006**, *16*, 685. (b) Maier, G. *Prog. Polym. Sci.* **2001**, *26*, 3. (c) Morgen, M.; Ryan, E. T.; Zhao, J.-H.; Hu, C.; Cho, T.; Ho, P. S. *Annu. Rev. Mater. Sci.* **2000**, *30*, 645. (d) Maex, K.; Baklanov, M. R.; Shamiryan, D.; Iacopi, F.; Brongersma, S. H.; Yanovitskaya, Z. S. *J. Appl. Phys.* **2003**, *93*, 8793.

(5) (a) Kim, Y.; Goh, W. H.; Chang, T.; Ha, C. S.; Ree, M. *Adv. Eng. Mater.* **2004**, *6*, 39. (b) Shin, T. J.; Ree, M. *Langmuir* **2005**, *21*, 6081. (c) Ree, M. *Macromol. Res.* **2006**, *14*, 1. (d) Azooz, M. A.; Hwang, Y. T.; Ree, M. *Egypt. J. Chem.* **2003**, *46*, 741. (e) Yu, J.; Ree, M.; Park, Y. H.; Shin, T. J.; Cai, W.; Zhou, D.; Lee, K.-W. *Macromol. Chem. Phys.* **2000**, *201*, 491. (f) Kim, S. I.; Ree, M.; Shin, T. J.; Lee, C.; Woo, T.-H.; Rhee, S. B. *Polymer* **2000**, *41*, 5173. (g) Yu, J.; Ree, M.; Shin, T. J.; Wang, X.; Cai, W.; Zhou, D.; Lee, K.-W. *Polymer* **2000**, *41*, 169. (h) Yu, J.; Ree, M.; Shin, T. J.; Wang, X.; Cai, W.; Zhou, D.; Lee, K.-W. *J. Polym. Sci.: Polym. Phys.* **1999**, *37*, 2806. (i) Pyo, S. M.; Kim, S. I.; Shin, T. J.; Park, Y. H.; Ree, M. *J. Polym. Sci., Part A: Polym. Chem.* **1999**, *37*, 937. (j) Kim, Y.; Kang, E.; Kwon, Y. S.; Cho, W. J.; Chang, C.; Ree, M.; Chang, T.; Ha, C. S. *Synth. Met.* **1997**, *85*, 1399.

(6) (a) Oh, W.; Shin, T. J.; Ree, M.; Jin, M. Y.; Char, K. *Macromol. Chem. Phys.* **2002**, *203*, 791. (b) Oh, W.; Ree, M. *Langmuir* **2004**, *20*, 6932.

(7) Ree, M.; Goh, W. H.; Kim, Y. *Polym. Bull.* **1995**, *35*, 215.

(8) (a) Lee, B.; Park, Y.-H.; Hwang, Y.-T.; Oh, W.; Yoon, J.; Ree, M. *Nat. Mater.* **2005**, *4*, 147. (b) Huang, E.; Toney, M. F.; Volksen, W.; Mecerreyes, D.; Brock, P.; Kim, H.-C.; Hawker, C. J.; Hedrick, J. L.; Lee, V. Y.; Magbitang, T.; Miller, R. D. *Appl. Phys. Lett.* **2002**, *81*, 2232. (c) Kim, H.-C.; Volksen, W.; Miller, R. D.; Huang, E.; Yang, G.; Briber, R. M.; Shin, K.; Satija, S. K. *Chem. Mater.* **2003**, *15*, 609.

(9) (a) Hedrick, J. L.; Miller, R. D.; Hawker, C. J.; Carter, K. R.; Volksen, W.; Yoon, D. Y.; Trollsas, M. *Adv. Mater.* **1998**, *10*, 1049.

(10) (a) Bolze, J.; Ree, M.; Youn, H. S.; Chu, S.-H.; Char, K. *Langmuir* **2001**, *17*, 6683. (b) Oh, W.; Hwang, Y.-T.; Park, Y. H.; Ree, M.; Chu, S.-H.; Char, K.; Lee, J.-K.; Kim, S. Y. *Polymer* **2003**, *44*, 2519.

(11) (a) Lee, B.; Oh, W.; Yoon, J.; Hwang, Y.; Kim, J.; Landes, B. G.; Quintana, J. P.; Ree, M. *Macromolecules* **2005**, *38*, 8991. (b) Lee, B.; Yoon, J.; Oh, W.; Hwang, Y.-T.; Heo, K.; Jin, K. S.; Kim, J.; Kim, K.-W.; Ree, M. *Macromolecules* **2005**, *38*, 3395.

(12) Lee, B.; Oh, W.; Hwang, Y.; Park, Y.-H.; Yoon, J.; Jin, K. S.; Heo, K.; Kim, J.; Kim, K.-W.; Ree, M. *Adv. Mater.* **2005**, *17*, 696.

(13) (a) Bolze, J.; Kim, J.; Huang, J.-Y.; Rah, S.; Youn, H. S.; Lee, B.; Shin, T. J.; Ree, M. *Macromol. Res.* **2002**, *10*, 2. (b) Lee, B.; Shin, T. J.; Lee, S. W.; Yoon, J.; Kim, J.; Ree, M. *Macromolecules* **2004**, *37*, 4174.

(14) Lee, B.; Park, I.; Yoon, J.; Park, S.; Kim, J.; Kim, K.-W.; Chang, T.; Ree, M. *Macromolecules* **2005**, *38*, 4311.

(15) (a) Kinning, D. J.; Thomas, E. L. *Macromolecules* **1984**, *17*, 1712. (b) Pedersen, J. S. *J. Appl. Crystallogr.* **1994**, *27*, 595.

(16) Young, R. J.; Lovell, P. A. *Introduction to Polymers*, 2nd ed.; Chapman & Hall: London, 1991; Chapter 3.

(17) Roe, R.-J. *Methods of X-ray and Neutron Scattering in Polymer Science*; Oxford University Press: New York, 2000.

(18) (a) Lee, H.-J.; Lin, E. K.; Wang, H.; Wu, W.-L., Chen, W.; Moyer, E. C. *Chem. Mater*. **2002**, *14*, 1845. (b) Yang, S.; Mirau, P. A.; Pai, C.-S.; Nalamasu, O.; Reichmanis, E.; Lin, E. K.; Lee, H.-J.; Gidley, D. W.; Sun, J. *Chem. Mater.* **2001**, *13*, 2762.

(19) (a) Balta-Calleja, F. J.; Vonk, C. G. *X-ray Scattering of Polymers*; Elsevier: Amsterdam, 1989. (b) Koberstein, J. T.; Stein, R. S. *J. Polym. Sci.: Polym. Phys. Ed.* **1983**, *21*, 2181. (c) Ruland, W. *J. Appl. Crystallogr.* **1971**, *4*, 70.